



Marcin Białas · Jan Maciejewski · Stanisław Kucharski

Friction coefficient of solid lubricating coating as a function of contact pressure: experimental results and microscale modeling

Received: 15 November 2020 / Accepted: 10 March 2021 / Published online: 8 April 2021
© The Author(s) 2021

Abstract The paper presents experimental analysis of relation between friction coefficient and contact pressure of MoS₂ film deposited on Ti₆Al₄V substrate in contact with sapphire ball during reciprocating sliding motion. It is shown that the value of friction coefficient decreases with increasing contact pressure. A microscale modeling approach is next developed to mimic the experimental observations. Representative volume element is defined based on the actual topography of outer surface of MoS₂ film. Assuming thermo-elastic material properties, the calculations on the asperity level are performed in two steps. Firstly, the mechanical contact between two surfaces is calculated. As a result, the relation between the global load and micro-stress distribution is obtained. Secondly, for a given stress load, thermal analysis is performed providing temperature fluctuation within simplified conical asperity. By assuming relation between friction coefficient and temperature on the microscale, it is possible to obtain macroscopic friction coefficient as a function of contact pressure. In the end, model results are compared with experimental data. The novel aspects of presented approach lie in the selection of three main factors on a micro-level defining macroscopic friction. They are actual surface topography, microscopic temperature and microscopic friction-temperature relation.

Keywords Microscale modeling · Friction coefficient · Flash temperature · Reciprocating motion test

1 Introduction

Surface asperities can lead to local concentration of contact pressure that can be orders of magnitude higher than observed macro-stress. The heat generated during frictional sliding is therefore concentrated on small contact spots. Its density in such areas can be very high. It results in short-time temperature elevation by hundreds of degrees. Because of that in tribology, it is common to distinguish three temperatures: the bulk temperature, the average surface temperature and the flash temperature. Bulk temperature is the temperature averaged over the bulk of one of the contacting bodies; surface temperature is the temperature averaged over the thin surface layer of a body; flash temperature is the local increment of temperature at the contact of micro-asperities on the rubbing surfaces. The notion of flash temperature reflects the discrete nature of frictional contact. The survey

Communicated by Marcus Aßmus, Victor A. Eremeyev and Andreas Öchsner.

M. Białas (✉)
Faculty of Production Engineering, Warsaw University of Technology, Warsaw, Poland
E-mail: marcin.bialas@pw.edu.pl

J. Maciejewski
Faculty of Automotive and Construction Machinery, Warsaw University of Technology, Warsaw, Poland

B. Kucharski
Institute of Fundamental Technological Research, Polish Academy of Sciences, Warsaw, Poland

of some existing solutions on temperature distribution within asperities in a microscale can be found in [1]. The authors discuss the influence of surface roughness on temperature and related phenomena like oxidation. In [2], a frequency domain thermoreflectance method is used to measure the thermal conductivity of a range of tribological materials. Calculations of maximum flash temperature rise are performed next.

There is a wide range of materials with shear stress showing high dependence on the applied normal loads. They are generally called friction-like or pressure sensitive materials, where different relations between friction coefficient and pressure on a macro-scale can be observed in experiments, see, for example, [3]. In the paper [4], effects of normal load on the measured friction coefficient by micro-scratch test with a spherical indenter were studied. A purely geometrical intersection model was used to rationalize the increase in the friction coefficient with increasing normal load. Maegawa et al. [5] studied the effect of normal load on the friction coefficient for sliding contact, and found the friction coefficient decreased with increasing load for rubber specimens. It is clearly seen that to properly understand qualitative mechanisms of frictional sliding, tribological considerations should be introduced into friction models. A brief survey of some of them is discussed in [6], and an experimental setup for identification of models material parameters is presented. In review paper [7], a total of 21 different friction force models are described and their fundamental physical and computational characteristics are discussed and compared in details. Authors conclude that both the choice of the friction model and its parameters can significantly affect the simulated response of mechanical systems. In [8], a strategy is proposed to characterize the friction behavior of materials of soft contact lenses by average work. The work is defined as the average value of a nonlinear function fitted to the friction versus normal force data, multiplied by a relevant sliding distance. In this way, the transition from coefficient of friction to work circumvents the necessity for a relationship between the lateral and normal forces and provides the energy dissipated when two interfaces slide over each other. Kumar et. al. [9] propose a unified framework accommodating the complex interdependence of the coefficient of friction, sliding velocity, axial pressure and temperature for implementation in response-history analyses performed on friction pendulum bearings in seismically isolated structures. Based on experimental data, the authors define the relationship between the coefficient of friction and sliding velocity, axial pressure and temperature. It turns out that frictional heating is the most important factor that influences the maximum displacement of the isolation system for high axial pressures. In the paper [10], Wang et al. study frictional behavior in dry metal forming. They show that the ratio of flattened area to smooth tool surface starts to increase sharply after the occurrence of bulk plastic deformation. To describe the observed response, they postulate a new friction law with constant friction coefficient at low contact pressure and associated frictional stress at high contact pressures. Nielsen and Bay [11] provide a concise summary of the most important contributions to friction modeling in metal forming since the early findings in adhesion theory around 1940 until the present state of the art. Many aspects are covered in the review: experimental techniques, upper bound solutions, slip-line analyses and numerical simulations. The paper highlights the importance of the real contact area and the influencing parameters including the material properties, surface conditions, normal pressure, sliding length and speed, temperature changes, friction on the flattened plateaus and plastic deformation in contact zones.

Since the area of real contact of bodies is one to three orders of magnitude lower than the nominal contact area, the solution of thermo-mechanical coupling on a macro-scale does not fully explain the wear process, oxidation and the variation of friction coefficient as a function of normal stress and temperature. Thus, it should be treated using two-scale modeling approach. The first scale is the macroscopic level, corresponding, for example, to ball-on-disc test, and the second scale is the asperity microscale level, see [12, 13]. Detailed overview of recent findings in the field of multi-scale modeling of contact phenomena can be found in [14]. The paper discusses surface representations, the breakdown of continuum theories at the nano- and microscales, as well as multi-scale and multiphysics aspects for analytical and computational models relevant to applications spanning a variety of sectors, from automotive to biotribology and nanotechnology. Localized deformation as a part of multi-scale modeling is discussed by Placidi et al. [15] and by Spagnuolo et al. [16]. As some material models do not seem suitable to describe the measured dissipation loops, Scerrato et al. [17] and Giorgio and Scerrato [18] propose to introduce a micro-mechanism of Coulombian internal dissipation associated with the relative motion of the lips of the micro-cracks present in the material. This microscale approach allowed for suitable description of some experimental evidences.

In [19], typical conditions are reviewed in which low friction coatings are sought as well as the demands for properties which coatings should fulfil in order to function in an appropriate way. An example of such coatings for use in a vacuum is based on molybdenum disulphide (MoS_2). Self-lubricating coatings with MoS_2 exhibit low friction and are used in the great majority of applications requiring solid lubrication. As examples, we could mention cutting tools such as drills and saws, highly loaded gear wheels made of titanium alloys,

sliding and roller bearings, cast iron pistons in radial piston motors, piston rings and home appliances including refrigerant compressors, washers and dryers.

The structure of MoS₂ is layered. Atoms belonging to one layer are strongly bonded by covalent interactions. There are van der Waals bonds between the layers which are weak and result in sliding at adjacent sulphur planes. Quasi-amorphous MoS₂Ti composite coatings, where Ti is added to molybdenum disulphide, are more adhesive, denser and more oxidation resistant than pure MoS₂. The effect of deposition parameters and Ti content on crystallographic orientation and friction coefficient and wear rate in MoS₂Ti was examined in [20]. The wear resistance and friction coefficient of the MoS₂Ti-coated Ti₆Al₄V alloy were investigated at various temperatures in the paper [21]. Review paper [22] compiles publications from last seventy years about the research developments in metal matrix self-lubricating composites containing MoS₂. Information on the tribological properties of such composites according to the varied matrixes, contents, processing conditions, testing temperatures and atmospheres is discussed.

The surface effects are important for modeling of some structures of nanofilms. In particular, they are responsible for the size effect, meaning the dependence of the material properties on the specimen size, issues relevant to thin films as MoS₂Ti coating. This problem is discussed by Altenbach and Eremeyev [23], where the theory of elasticity is applied to the modeling of shells with nano-scaled thickness. To capture the material behavior at the nanoscale, Eremeyev et al. [24] use linearized Gurtin–Murdoch surface elasticity approach and discuss the propagation of transverse surface waves along a surface of an elastic cylinder with coating. Authors provide other interpretations of the surface shear modulus.

The aim of present paper is to derive macroscopic relation between pressure and friction coefficient for sapphire ball sliding on MoS₂ film deposited on Ti₆Al₄V substrate. As a starting point, we show results of reciprocating motion experiments at specified amplitude and frequency (ball-on-flat-test) in unlubricated conditions. The experiments were done in room temperature. Ball/coating friction coefficient was measured as a function of mean contact pressure. Theoretical approach is developed next to mathematically describe the relation between friction and pressure observed during the experiments. It is based on microscale modeling. Representative volume element is chosen using the actual film surface topography. Assuming thermo-elastic material properties, the calculation on the asperity scale is performed in two steps. The first step is the calculation of mechanical contact within the representative element between the ball and the coating. As a result, the relation between the global load and micro-stress distribution is obtained. Next, for a given stress load finite element thermal analysis is performed providing temperature fluctuations on the asperity level. By assuming relation between friction coefficient and temperature on the microscale and applying averaging procedure, it is then possible to obtain macroscopic friction coefficient as a function of macroscopic contact pressure. Predictions of microscale modeling are compared with experimental data from reciprocating sliding test.

2 Reciprocating sliding test

A plate sample made of Ti₆Al₄V titanium alloy deposited with MoS₂ coating of thickness 3 μm was put in contact with a sapphire (Al₂O₃) ball of 6 mm diameter undergoing reciprocating sliding motion of specified amplitude and frequency (ball-on-flat-test) in unlubricated conditions. The topography of initial outer surface of MoS₂ layer was measured using a scanning profilometer Hommel Tester T8000 Nanoscan. All roughness parameters were determined using Hommel Map software for surface analysis. The following values were obtained: arithmetic mean deviation $R_a = 0.62 \mu\text{m}$, root-mean-squared deviation $R_q = 0.82 \mu\text{m}$, mean spacing of profile elements $S_m = 30 \mu\text{m}$, root-mean-squared slope of assessed profile $R_{dq} = 7.9^\circ$.

The reciprocating sliding tests were done in room temperature using homemade wear tester. The ball was loaded with different values of normal forces pressing it to the substrate. For each load, a reciprocating motion was imposed with 100 cycles and stroke length of 3 cm. The value of sliding force was recorded. The frequency of ball oscillation was 3.33 s^{-1} and did not change for all the tests. It was not intended to examine the effect of sliding velocity on frictional response. The experimental setup is illustrated in Fig. 1.

The friction coefficient was measured as a ratio of tangential and normal forces at the contacted surfaces. Assuming Hertz contact conditions under the ball, the mean pressure was calculated for each normal loading using formula $F/(\pi a^2)$, where F is the normal force and a is radius of contact zone given by

$$a^3 = \frac{3}{4} F R \left(\frac{1 - \nu_1^2}{E_1} + \frac{1 - \nu_2^2}{E_2} \right). \quad (1)$$

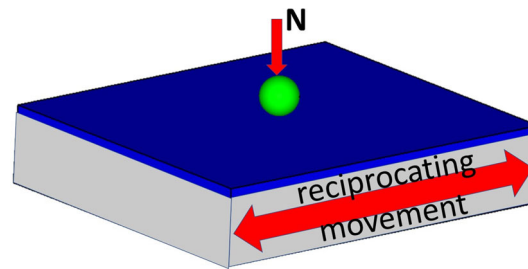


Fig. 1 Reciprocating test with 100 cycles and a stroke length of 3 cm. Frequency of oscillation was 3.33 s^{-1} . Different loading forces were applied

Table 1 Material parameters of MoS₂ layer (after [25] and [26])

Young modulus	Poisson's ratio	Density	Specific heat	Thermal conductivity	Thermal expansion coefficient
200 GPa	0.3	$5.06 \frac{\text{g}}{\text{cm}^3}$	$1.81 \frac{\text{J}}{\text{cm}^3 \text{ K}}$	$0.6 \frac{\text{W}}{\text{m K}}$	$8.65 \cdot 10^{-6} \frac{1}{\text{C}}$

Table 2 Material parameters of Al₂O₃ ball

Young modulus	Poisson's ratio	Density	Specific heat	Thermal conductivity	Thermal expansion coefficient
380 GPa	0.3	$3.89 \frac{\text{g}}{\text{cm}^3}$	$0.88 \frac{\text{J}}{\text{g K}}$	$30 \frac{\text{W}}{\text{m K}}$	$8.1 \cdot 10^{-6} \frac{1}{\text{C}}$

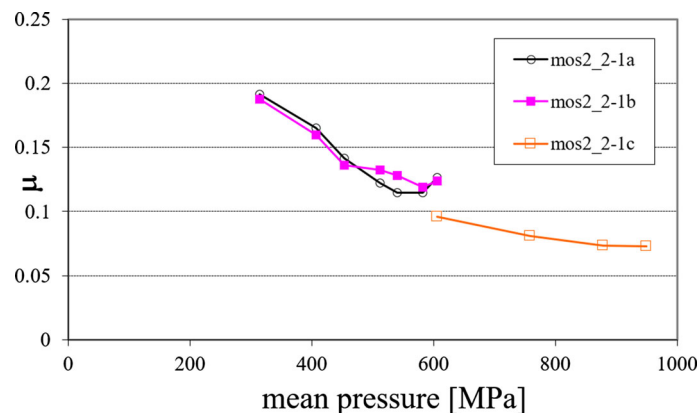


Fig. 2 Reciprocating test. Friction coefficient as a function of Hertz mean contact pressure

In the above equation, R is ball radius, E_1 , ν_1 , E_2 , ν_2 are Young's modulus and Poisson's ration of the MoS₂ layer and the sapphire ball, see Tables 1 and 2, respectively.

Figure 2 presents obtained friction coefficient as a function of mean contact pressure. Two sets of tests were performed for loading forces 0.24 N, 0.51 N, 0.71 N, 1.02 N, 1.20 N, 1.49 N, 1.69 N: tests (a) and (b). The third set of tests was done for forces 1.69 N, 3.31 N, 5.14 N, 6.47 N: test (c). In general, it can be stated that friction coefficient decreases from 0.19 to 0.07 as the mean contact pressure increases from 314 to 949 MPa. Only for loading force of 1.69 N applied during tests (a) and (b), a slight increase in the friction coefficient was observed. Because of that the same force was used during test (c) and the results for 1.69 N showed expected correlation with other loadings applied during tests (a) and (b). For mean pressures in the range 900–1000 MPa friction coefficient stabilizes around value of 0.073.

3 Microscale friction model

The surface topography of MoS₂ film obtained from scanning profilometer is used to build geometry of the finite element model of a representative film and substrate volume with the typical roughness profile. Its

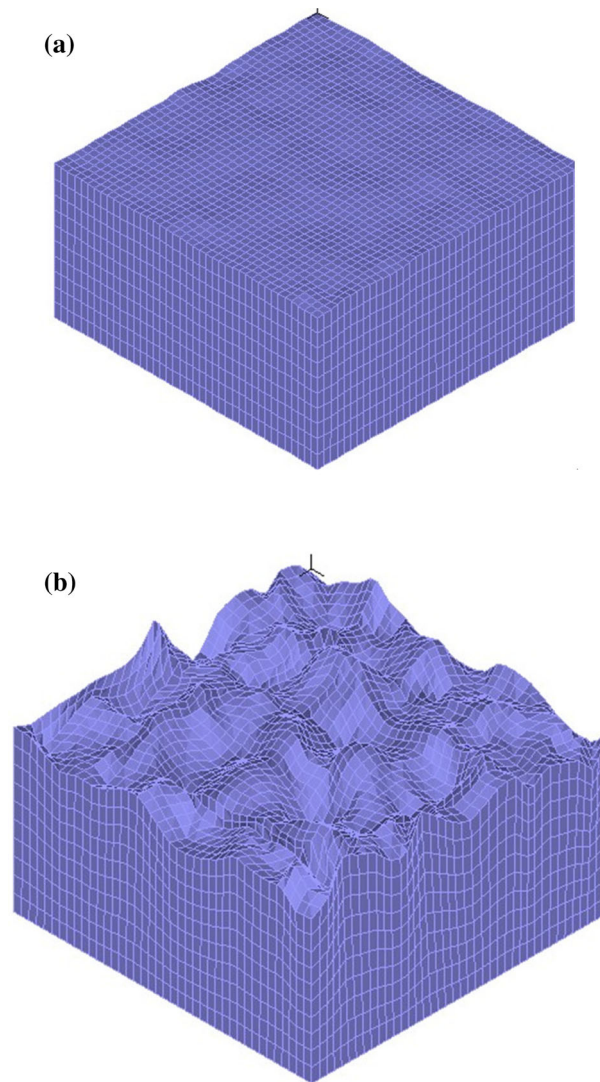


Fig. 3 **a** Mesh of the representative volume element. **b** Mesh scaled twenty times in vertical direction to magnify asperities profile

dimensions $200 \times 200 \mu\text{m}$ are taken to be sufficiently large for the unit cell not to be affected by the finite size. The height of the model is $100 \mu\text{m}$ with $3 \mu\text{m}$ film thickness. Figure 3a depicts the 3D mesh approximation. Figure 3b shows mesh scaled twenty times in vertical direction to magnify the roughness profile.

The following calculation scheme is applied for the micro-level, providing us at the end with the relation between macroscopic contact stress and the friction coefficient. It is achieved by taking into account temperature fluctuations on the asperity level.

- (1) *Obtain local stress* By pressing a rigid flat surface against the representative volume element of film deposited on the substrate, we calculate local normal contact stresses σ^{micro} and the resulting mean normal traction acting on the upper MoS_2 surface

$$\sigma = \frac{1}{A_0} \int_{A_0} \sigma^{\text{micro}} dA_0. \quad (2)$$

Both σ^{micro} and σ depend on the real contact area A_r between the element and the pressing object. It can be characterized by parameter α , $0 \leq \alpha \leq 1$, being the ratio between A_r and the nominal surface area A_0

$$\alpha = \frac{A_r}{A_0}, \quad (3)$$

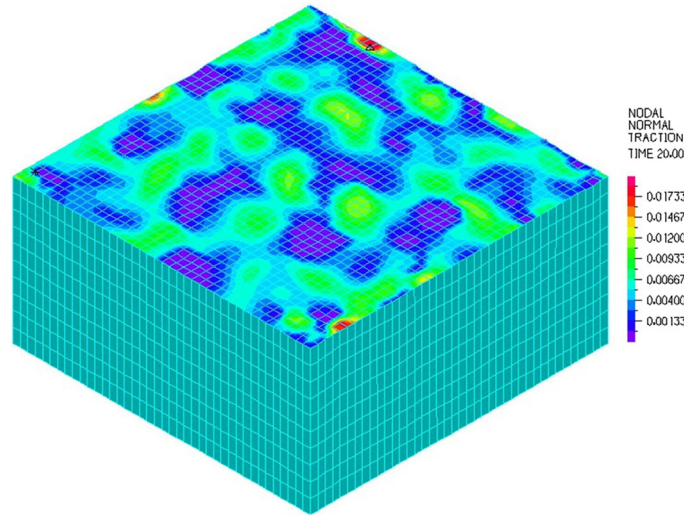


Fig. 4 Nodal forces [N] within the representative element for $\alpha = 0.4$

where in our case $A_0 = 200\mu\text{m} \times 200\mu\text{m}$. Periodic boundary conditions (zero horizontal displacements) are imposed on the sides of the representative element, and the bottom surface is fixed. The calculated σ in formula (2) is simply normal contact traction on the macro-scale: For given macro-scale σ , we can establish the real contact area for our particular surface topography presented in Fig. 3.

Exemplary results of nodal forces within the representative element for $\alpha = 0.4$ are presented in Fig. 4. One can see non-uniform nodal force distribution and peaks in pressing traction due to real topography. The overall picture depicts very irregular shape of real contact area. Nodal forces can be used next to calculate maximum, mean and average contact pressure within the representative element as a function of real contact area described by parameter α . This is presented in Fig. 5. Mean stress is given by Eq. (2) and shows the value of loading force divided by nominal contact area $\sigma_{\text{mean}} = F/A_0$. It is in fact the stress level observed at the macroscopic scale during the pressing process. Average stress is the loading force divided by real contact area $\sigma_{\text{ave}} = F/A_r$ and can be followed during numerical calculations. It should be noticed that the maximum normal stress acting on the representative area is much higher than its mean counterpart. For example, for $\alpha = 0.4$ the maximum stress is 4494 MPa and the mean stress is 433 MPa, so the difference is one order of magnitude. It clearly shows that on the micro-level, one can expect local phenomena to happen which are not captured on macro-scale after averaging procedure.

- (2) *Obtain local heat flux* Knowing the distribution of local σ^{micro} for a given α , we calculate the resulting local heat flux

$$q^{\text{micro}} = f \tau^{\text{micro}} v = f \mu^{\text{micro}}(T^{\text{micro}}) \sigma^{\text{micro}} v \quad (4)$$

when the representative element slides against the contacting body with relative velocity v . In the above equation, $f = 0.5$ is the fraction of the dissipated energy absorbed by the volume element of MoS_2 layer. It means that the remaining part of the energy goes into the pressing object. It is assumed that the sliding velocity on the micro-level is uniform and has the same value as its macroscopic counterpart. The relation between the local friction coefficient and local temperature is assumed to have the form

$$\mu^{\text{micro}}(T^{\text{micro}}) = \mu_{\text{max}}^{\text{micro}} - \left(\mu_{\text{max}}^{\text{micro}} - \mu_{\text{min}}^{\text{micro}} \right) \left(\frac{T^{\text{micro}} - T_{\text{min}}^{\text{micro}}}{T_{\text{max}}^{\text{micro}} - T_{\text{min}}^{\text{micro}}} \right)^7 \quad (5)$$

As presented in Fig. 6, it decreases from $\mu_{\text{max}}^{\text{micro}}$ to $\mu_{\text{min}}^{\text{micro}}$ as temperature changes from $T_{\text{min}}^{\text{micro}}$ up to $T_{\text{max}}^{\text{micro}}$.

- (3) *Obtain local temperature* The resulting heat flux q^{micro} gives rise to a steady-state temperature increase ΔT^{micro} above the initial temperature T^{init} within the volume element. Locally, the sum

$$T^{\text{micro}} = T^{\text{init}} + \Delta T^{\text{micro}} \quad (6)$$

can be greater than the averaged temperature

$$T = \frac{1}{A_0} \int_{A_0} T^{\text{micro}} dA_0 \quad (7)$$

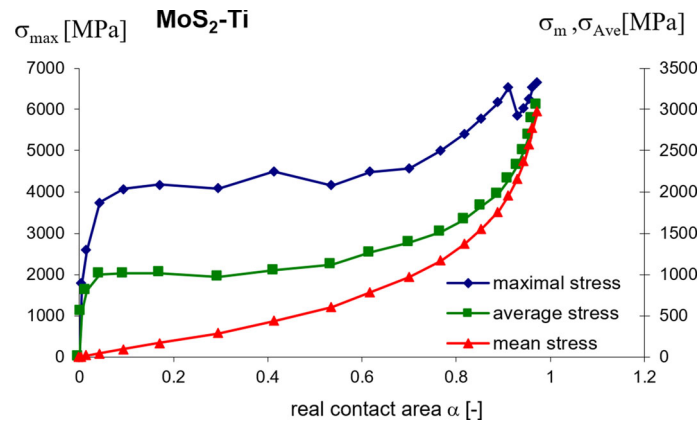


Fig. 5 Maximum, average and mean stresses acting on representative element as a function of fraction of real contact area $\alpha = A_r/A_0$

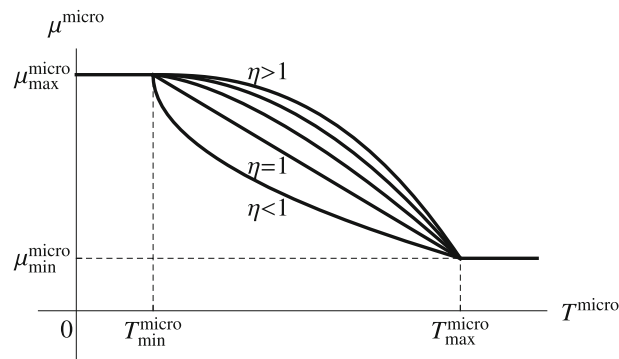


Fig. 6 Relation between local friction coefficient and local temperature

on the upper surface on the macro-scale. The calculation of temperature T^{micro} should be performed by assuming periodic boundary conditions, that is, zero heat flow through the vertical boundaries of the representative element. Its height should be big enough for temperature fluctuations to occur only close to its upper surface.

- (4) *Calculate macroscopic friction coefficient* By definition the macroscopic friction coefficient is the ratio of macroscopic tangential and normal forces

$$\mu(T, \sigma) = \frac{\int_{A_0} \tau^{\text{micro}} dA_0}{\int_{A_0} \sigma^{\text{micro}} dA_0}, \quad (8)$$

where the integration is done over the upper surface of the representative element. It should be noticed that the local relation (5) between temperature and friction coefficient is transformed now and provides us with a macroscopic μ being the function of macroscopic temperature and macroscopic normal contact stress.

Temperature T in the definition of macroscopic friction coefficient (8) is the averaged temperature on the upper surface of the representative element, directly between the contacting bodies. It is difficult to be measured experimentally, and for practical reasons, it is better to use T^{init} instead of T when comparing model results with available experimental data. The value of T^{init} can be interpreted as ambient temperature of a tribological test.

To effectively calculate integrals in (7) and (8), a simplified representative element has been chosen with external loading equivalent to real topography situation. It consists of a single conical asperity as presented in Fig. 7. The upper surface is equal to the real contact area A_r ; the area of bottom surface has the nominal value $A_0 = 40,000 \mu\text{m}^2$. It is in line with original cubic representative volume element where horizontal dimensions are $200 \times 200 \mu\text{m}$. The height of $100 \mu\text{m}$ is the same as previously assumed for the volume with real topography.

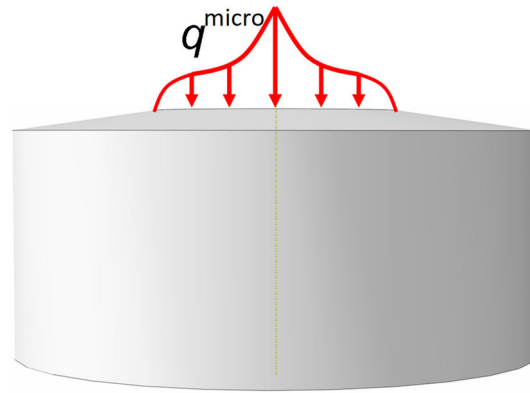


Fig. 7 Simplified representative element: single conical asperity

Table 3 Material parameters of $\text{Ti}_6\text{Al}_4\text{V}$ substrate (after [27])

Young modulus	Poisson's ratio	Density	Specific heat	Thermal conductivity	Thermal expansion coefficient
110 GPa	0.31	$4.42 \frac{\text{g}}{\text{cm}^3}$	$553 \frac{\text{J}}{\text{kg K}}$	$7.1 \frac{\text{W}}{\text{m K}}$	$9.2 \cdot 10^{-6} \frac{1}{\text{C}}$

Axisymmetric contact loading σ^{micro} applied to the simplified conical element satisfies the following conditions: It reaches its maximal value $\sigma_{\text{max}}^{\text{micro}}$ on the symmetry axis and monotonically decreases to zero on the boundary of the real contact zone. Micro-stresses presented in Fig. 5 provide input needed to properly evaluate equivalent loading applied to the simplified representative element. The distribution of σ^{micro} acting on the single conical asperity was chosen so that the area covered by σ^{micro} bounded by $\sigma_i < \sigma^{\text{micro}} < \sigma_{i+1}$ is the same both for the simplified and the real topography volume elements. The number of divisions J , where we have

$$0 = \sigma_1 < \dots < \sigma_j < \dots < \sigma_J = \sigma_{\text{max}}^{\text{micro}},$$

was $J = 10$, to ensure that the external loading imposed on the simplified element is equivalent to that acting on the real topography.

4 Model results and discussion

The relevant material parameters of MoS_2 film, the ball and $\text{Ti}_6\text{Al}_4\text{V}$ substrate are listed, respectively, in Tables 1, 2 and 3. For micro-scale relation between the friction coefficient and temperature, we assume in Eq. (5): $\mu_{\text{max}}^{\text{micro}} = 0.2$, $\mu_{\text{min}}^{\text{micro}} = 0.05$, $T_{\text{max}}^{\text{micro}} = 200^\circ\text{C}$, $T_{\text{min}}^{\text{micro}} = 0^\circ\text{C}$, $\eta = 1$. It roughly matches with experimental data presented by Kubart et al. [28]

Figure 8 presents the obtained distribution of normal contact stresses on the axisymmetric representative element for various values of nominal contact area. It was obtained from real topography stresses by the procedure described above. Obviously for higher value of α , that is for bigger nominal contact area, the pressure increases, with its peak value reached on the symmetry axis of the representative element. By application of (4), the pressure is related to shear stress and results in heat flux arising due to friction when the ball is sliding over the disc. It has to be noted that heat flux depends on temperature values at contact zone of the representative element through relation $\mu^{\text{micro}}(T^{\text{micro}})$ given by Eq. (5). In order to properly calculate combined effect of applied heat flux and resulting temperature distribution within the asperity, ABAQUS user subroutine DFLUX was coded, see [29]. It can be used to define a nonuniformly distributed flux as a function of temperature in a heat transfer analysis.

Temperature distribution obtained as a steady-state solution to heat flow problem is presented in Fig. 9 for nominal contact area $\alpha = 0.016$, $\alpha = 0.4$ and $\alpha = 0.89$. Ambient temperature was set to 20°C . The notion of flash temperature can be seen for $\alpha = 0.016$ and $\alpha = 0.4$, with its value significantly higher in a localized contact zone, where it varies from 150 to 190°C , depending on nominal contact area. It can lead to local oxidation phenomena not captured by typical consideration, where microscale modeling aspects are

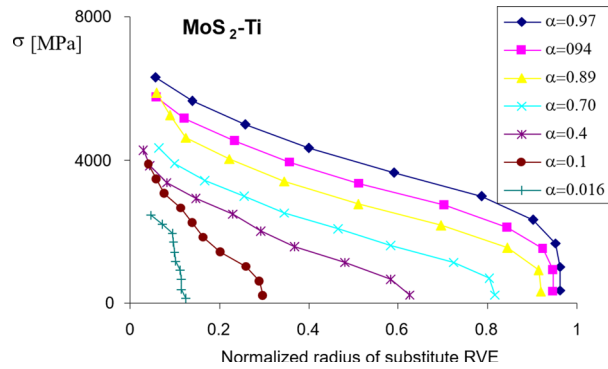


Fig. 8 Distribution of normal contact stresses on the conical representative element of contact zone for various values of parameter α depicting nominal contact area

excluded, as preliminary reported in [30]. Bulk temperature is much smaller with values between 20 and 35 °C predominant within the examined volume. For $\alpha = 0.89$, that is for almost all upper surface of the representative element being in contact with the pressing object, the effect of flash temperature disappears, as heat flux is not imposed on a localized area in this case. The variation of T^{micro} on the upper surface of the representative element is presented in Fig. 10 for several values of α . It can be observed that already for nominal contact area $\alpha \geq 0.1$ maximum values of temperature on the symmetry axis do not change much with increasing α . They asymptotically tend to reach 195 °C for α close to unity. For higher values of nominal contact area, the temperature becomes uniform on most of the upper surface.

Figure 11 presents macroscopic friction coefficient μ as a function of macroscopic σ for surrounding temperature of 20 °C. It was obtained by the use of relation (8), where integration was done over simplified representative asperity with flash temperature obtained as explained above. Simulation results are compared with values of μ measured experimentally during reciprocating test described in Sect. 2. We can see that the general experimental trend is preserved by the multi-scale modeling approach: Coefficient is decreasing as the stress is increasing. It varies mostly for lower values of contact pressure. Although simulation results are not ideally matching, they can be used as a rough approximation of experimental data. Proposed multi-scale approach explains the complex aspects of variation of μ for different loading conditions. It shows that friction coefficient is affected by the height of the asperity and the resulting temperature distribution on the micro-level, when two bodies are in sliding contact. The model is also open for subsequent improvements. On microscale, the ball was modeled as a flat rigid surface and its surface topography was not taken into account when calculating contact pressure. By pressing two elastic-plastic bodies with real surface topography on both contact surfaces, one could obtain better approximation of local stresses. In addition, the microscale relation (5) between local friction coefficient and local temperature is the input to the proposed modeling. This could be modified to better capture physics of contact phenomena. By using the proposed approach, it is also straightforward to obtain value of friction coefficient as a function of sliding speed. The relative velocity between two contacting bodies is already present in the formula (4), providing heat flux acting on contact area of asperity. As a result, the macroscopic friction coefficient defined by averaging Eq. (8) can also be expressed in terms of sliding speed.

5 Summary and conclusions

Experimental results of room-temperature reciprocating sliding motion at specified amplitude and frequency (ball-on-flat-test) in unlubricated conditions are reported for sapphire ball in contact with MoS₂ film deposited on Ti₆Al₄V. They are used to calculate friction coefficient for various values of ball loading force. It is shown that with increasing ball loading and subsequently increasing contact pressure, the value of friction coefficient becomes lower.

Microscale model is developed to obtain relation between macroscopic pressure and macroscopic friction coefficient. Due to surface roughness in the contact zone, we have areas where the ball sticks to the film and those where they are separated. In the microscale, this leads to stress and temperature concentrations. This is known in the literature as flash temperature: highly localized temperature in the peaks of asperities. This is a microscale effect. By averaging pressure and shear stresses at contact within representative element, we can in

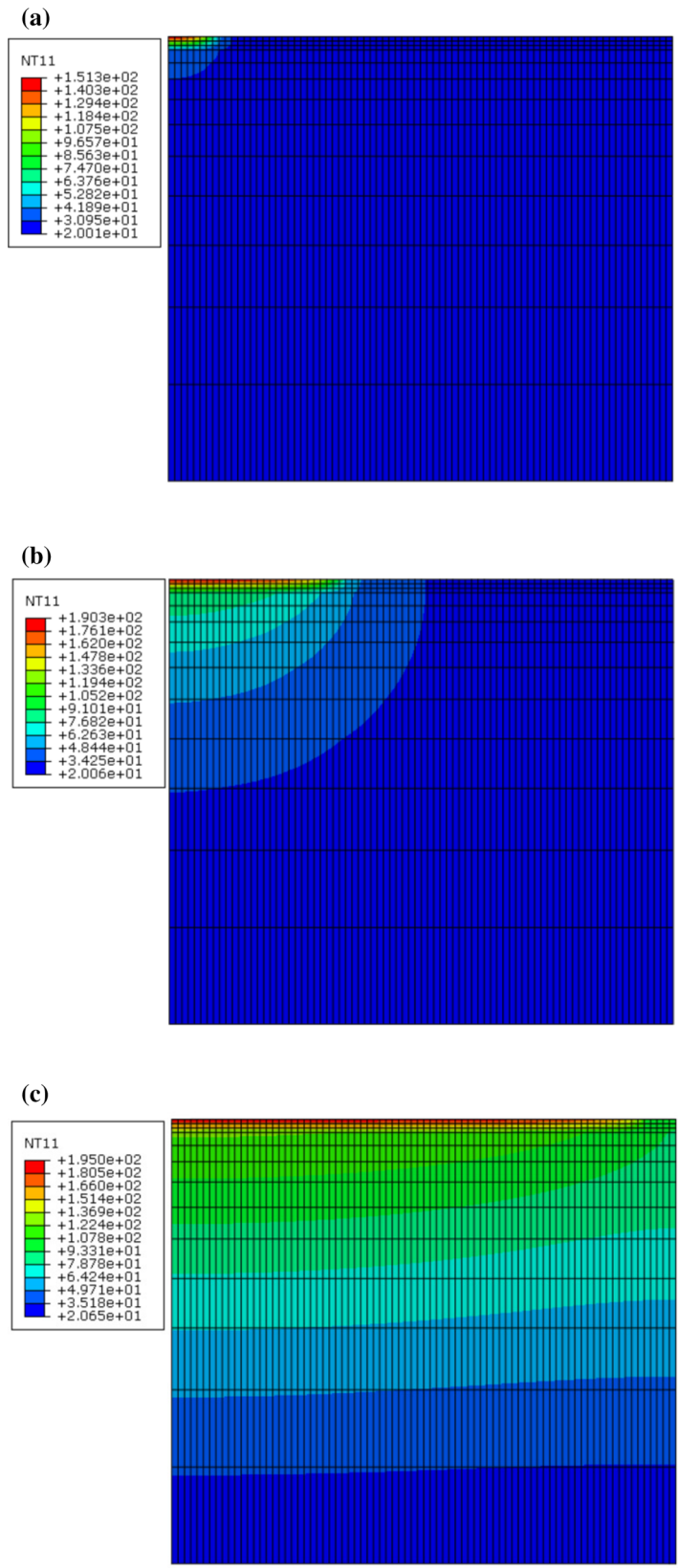


Fig. 9 Temperature distribution within the conical representative element for **a** $\alpha = 0.016$, **b** $\alpha = 0.4$, **c** $\alpha = 0.89$

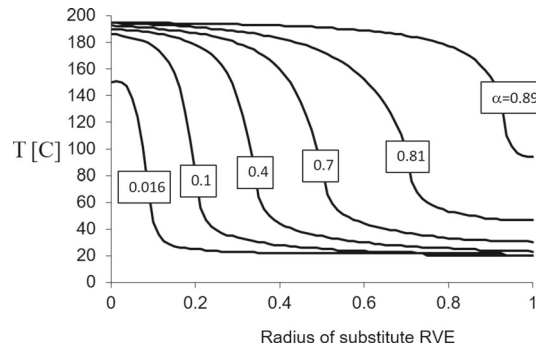


Fig. 10 Temperature distribution over the contact surface of conical representative element for various values of α

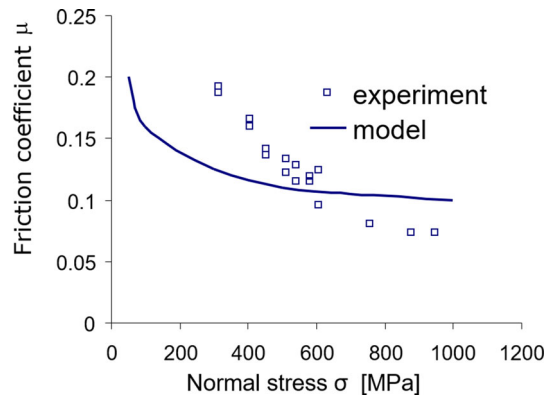


Fig. 11 Macroscopic friction coefficient as a function of average normal stress for ambient temperature of 20 °C: experiment versus model results

turn obtain macroscopic friction coefficient as a function of normal stress. In this way, the nonlinear relation $\mu(\sigma)$ is a result and not an a priori assumption. It arises due to temperature fluctuation within the asperity and consequent nonlinear character between normal and shear microscopic stresses

$$\tau^{\text{micro}} = \mu^{\text{micro}}(T^{\text{micro}})\sigma^{\text{micro}}, \quad (9)$$

where $\mu^{\text{micro}}(T^{\text{micro}})$ is given by equation (5). As can be seen, the ratio of averaged values of σ^{micro} and τ^{micro} is therefore not constant. The results of the model are compared to experimental findings in terms of relation between friction coefficient and pressure. Although simulation results are not ideally matching, they can be used as a rough approximation of experimental data.

The novel aspects of presented approach lie in the selection of three main factors on a micro-level that will define macroscopic friction. They are actual surface topography, microscopic temperature and microscopic friction-temperature relation. Future research could combine this multi-scale model with simulating material wear accompanying sliding between contacting bodies. Oxidation modeling is another research direction to follow. When calculating flash temperature, it is clearly seen that its value on asperities can be orders of magnitude higher than its macroscopic counterpart. By integrating microscale oxidation activation factors dependent on distribution of local temperatures, it would be possible to capture formation of oxide layer. This task might not be possible within conventional approach, where macroscopic temperature could be below a macroscopic threshold value for oxidation initiation.

The tools presented in this work can be used for accurate evaluation of friction-related relations in damage evolution problems [31,32] and can allow for a better insight into hysteresis phenomena occurring during frictional sliding between several mechanical components [33]. They could also serve as a microscale input for contact rules proposed on the macro-scale [34] or be used in the research trend on generalized continua such as pantographic structures [35], where rotating joints are affected by frictional sliding.

Acknowledgements This work was supported by Polish Ministry of Science and Education, contr.no. POIG.01.03.01-14-013/08-00 within the project KomCerMet.

Open Access This article is licensed under a Creative Commons Attribution 4.0 International License, which permits use, sharing, adaptation, distribution and reproduction in any medium or format, as long as you give appropriate credit to the original author(s) and the source, provide a link to the Creative Commons licence, and indicate if changes were made. The images or other third party material in this article are included in the article's Creative Commons licence, unless indicated otherwise in a credit line to the material. If material is not included in the article's Creative Commons licence and your intended use is not permitted by statutory regulation or exceeds the permitted use, you will need to obtain permission directly from the copyright holder. To view a copy of this licence, visit <http://creativecommons.org/licenses/by/4.0/>.

References

1. Bogdanovich, P., Tkachuk, D.: Thermal and thermomechanical phenomena in sliding contact. *J. Frict. Wear.* **30**, 153–163 (2009)
2. Reddyhoff, T., Schmidt, A., Spikes, H.: Thermal conductivity and flash temperature. *Tribol. Lett.* **67**, 22 (2019)
3. Bilotta, A., Turco, E.: Elastoplastic analysis of pressure-sensitive materials by an effective three-dimensional mixed finite element model. *Z. Angew. Math. Mech.* **97**, 382–396 (2017)
4. Gao, C., Liu, M.: Effects of normal load on the coefficient of friction by microscratch test of copper with a spherical indenter. *Tribol. Lett.* **67**, 8 (2019)
5. Maegawa, S., Itoigawa, F., Nakamura, T.: Effect of normal load on friction coefficient for sliding contact between rough rubber surface and rigid smooth plane. *Tribol. Int.* **92**, 335–343 (2015)
6. Sun, Y.-H., Chen, T., Qiong, Wu, C., Shafai, C.: A comprehensive experimental setup for identification of friction model parameters. *Mech. Mach. Theory* **100**, 338–357 (2016)
7. Marques, F., Flores, P., Claro, P., Lankarani, H.: A survey and comparison of several friction force models for dynamic analysis of multibody mechanical systems. *Nonlinear Dyn.* **86**, 1407–1443 (2016)
8. Sterner, O., Aeschlimann, R., Zürcher, S., Scales, C., Riederer, D., Spencer, N.D., Tosatti, S.: Tribological classification of contact lenses: from coefficient of friction to sliding work. *Tribol. Lett.* **63**, 9 (2016)
9. Kumar, M., Whittaker, A., Constantinou, M.: Characterizing friction in sliding isolation bearings. *Earthq. Eng. Struct. Dyn.* **44**(9), 1409–1425 (2015)
10. Wang, Z.G., Yoshikawa, Y., Suzuki, T., Osakada, K.: Determination of friction law in dry metal forming with DLC coated tool. *CIRP Ann.* **63**(1), 277–280 (2014)
11. Nielsen, C., Bay, N.: Review of friction modeling in metal forming processes. *J. Mater. Process. Technol.* **255**, 234–241 (2018)
12. Luongo, A., D'Annibale, F.: Modeling the linear dynamics of continuous viscoelastic systems on their infinite-dimensional central subspace. *Math. Mech. Complex Syst.* **8**(2), 127–151 (2020)
13. Lengiewicz, J., Stupkiewicz, S.: Continuum framework for finite element modelling of finite wear. *Comput. Method Appl. Mech. Eng.* **205–208**, 178–188 (2012)
14. Vakis, A., Yastrebov, V., Scheibert, J., Nicola, L., Dini, D., Minfray, C., Almqvist, A., Paggi, M., Lee, S., Limbert, G., Molinari, J., Ancaix, G., Aghababaei, R., Echeverri Restrepo, S., Papangelo, A., Cammarata, A., Nicolini, P., Putignano, C., Carbone, G., Stupkiewicz, S., Lengiewicz, J., Costagliola, G., Bosia, F., Guarino, R., Pugno, N., Mueser, M., Ciavarella, M.: Modeling and simulation in tribology across scales: an overview. *Tribol. Int.* **125**, 169–199 (2018)
15. Placidi, L., Barchiesi, E., Misra, A.: A strain gradient variational approach to damage: a comparison with damage gradient models and numerical results. *Math. Mech. Complex Syst.* **6**(2), 77–100 (2018)
16. Spagnuolo, M., Barcz, K., Pfaff, A., dell'Isola, F., Franciosi, P.: Qualitative pivot damage analysis in aluminum printed pantographic sheets: numerics and experiments. *Mech. Res. Commun.* **83**, 47–52 (2017)
17. Scerrato, D., Giorgio, I., Madeo, A., Limam, A., Darve, F.: A simple non-linear model for internal friction in modified concrete. *Int. J. Eng. Sci.* **80**, 136–152 (2014)
18. Giorgio, I., Scerrato, D.: Multi-scale concrete model with rate-dependent internal Friction. *Eur. J. Environ. Civ. Eng.* **21**, 821–839 (2017)
19. Hirvonen, J.-P., Koskinen, J., Jervis, J., Nastasi, M.: Present progress in the development of low friction coatings. *Surf. Coat. Technol.* **80**(1–2), 139–150 (1996)
20. Arlsan, E., Buelbuel, F., Alsaran, A., Celik, A., Efeoglu, I.: The effect of deposition parameters and Ti content on structural and wear properties of MoS₂Ti coatings. *Wear* **259**(7–12), 814–819 (2005)
21. Moskalewicz, T., Zimowski, S., Wendler, B., Nolbrzak, P., Czyska-Filemonowicz, A.: Microstructure and tribological properties of low-friction composite MoS₂(Ti, W) coating on the oxygen hardened Ti-6Al-4V alloy. *Met. Mater. Int.* **20**, 269–276 (2014)
22. Furlan, K., de Mello, J., Klein, A.: Self-lubricating composites containing MoS₂: a review. *Tribol. Int.* **120**, 280–298 (2018)
23. Altenbach, H., Eremeyev, V.A.: On the shell theory on the nanoscale with surface stresses. *Int. J. Eng. Sci.* **49**(12), 1294–1301 (2011)
24. Eremeyev, V.A., Rosi, G., Naili, S.: Transverse surface waves on a cylindrical surface with coating. *Int. J. Eng. Sci.* **147**, 103188 (2020)
25. McLaren, R.: Thermal conductivity anisotropy in molybden disulfide thin films. Ph.D. thesis, University of Illinois at Urbana-Champaign, Urbana, Illinois (2009)
26. Donnet, C., Martin, J., Le Mogne, T., Belin, M.: Super-low friction of MoS₂ coatings in various environments. *Tribol. Int.* **29**(2), 123–128 (1996)
27. Murr, L., Esquivel, E., Quinones, S., Gaytan, S., Lopez, M., Martinez, E., Medina, F., Hernandez, D., Martinez, E., Martinez, J., Stafford, S., Brown, D., Hoppe, T., Meyers, W., Lindhe, U., Wicker, R.: Microstructures and mechanical properties of electron beam-rapid manufactured Ti-6Al-4V biomedical prototypes compared to wrought Ti-6Al-4V. *Mater. Charact.* **60**(2), 96–105 (2009)

28. Kubart, T., Polcar, T., Kopecký, L., Novák, R., Nováková, D.: Temperature dependance of tribological properties of MoS₂ and MoSe₂ coatings. *Surf. Coat. Technol.* **193**(1–3), 230–233 (2005)
29. Deassault Systèmes: ABAQUS version 6.7, User documentation (2007)
30. Maciejewski, J., Białas, M., Mróz, Z.: Modelling of contact interface oxidation process at asperity scale. In: *Proceeding of 6th European Congress on Computational Methods in Applied Sciences and Engineering (ECCOMAS 2012)*, pp. 1–8 (2012)
31. Placidi, L., Misra, A., Barchiesi, E.: Two-dimentional strain gradient damage modelling: a variational approach. *Z. Angew. Math. Phys.* **69**, 56 (2018)
32. Volkov, I.A., Igumnov, L.A., dell’Isola, F., Litvinchuk, S.Y., Eremeyev, V.A.: A continual model of a damaged medium used for analyzing fatigue life of polycrystalline structural alloys under thermal-mechanical loading. *Contin. Mech. Thermodyn.* **32**, 229–245 (2020)
33. Vaiana, N., Sessa, S., Marmo, F., Rosati, L.: A class of uniaxial phenomenological models for simulating hysteretic phenomena in rate-independent mechanical systems and materials. *Nonlinear Dyn.* **93**(3), 1647–1669 (2018)
34. Cuomo, M., Ventura, G.: Complementary energy approach to contact problems based on consistent augmented Lagrangian formulation. *Math. Comput. Model.* **28**(4–8), 185–204 (1998)
35. Giorgio, I., Ciallella, A., Scerrato, D.: A study about the impact of the topological arrangement of fibers on fiber-reinforced composites: some guidelines aiming at the development of new ultra-stiff and ultra-soft metamaterials. *Int. J. Solids Struct.* **203**, 73–83 (2020)

Publisher’s Note Springer Nature remains neutral with regard to jurisdictional claims in published maps and institutional affiliations.